ETCHING OF HIGH PURITY ZINC

R. C. BRANDT, K. H. ADAMS AND T. VREELAND, JR.

DECEMBER 1961

A REPORT ON RESEARCH CONDUCTED UNDER CONTRACT WITH THE OFFICE OF NAVAL RESEARCH

W. M. KECK LABORATORY OF
ENGINEERING MATERIALS

CALIFORNIA INSTITUTE OF TECHNOLOGY

PASADENA

ETCHING OF HIGH PURITY ZINC

By

R. C. Brandt, K. H. Adams, T. Vreeland, Jr.

First Technical Report
under
Office of Naval Research
Contract No. Nonr-220(37)
Task No. NR 031-677

California Institute of Technology
Pasadena, California

December 1961

ETCHING OF HIGH PURITY ZINC

Table of Contents

LIST OF FIGURES

ABSTRACT

An etching technique for revealing dislocations in high purity zinc single crystals without the addition of solute impurities has been developed. The technique involves surface doping prior to chemical polishing. Evidence for a one to one correspondence between etch figures and dislocations is presented, together with some preliminary observations of slip on (0001) basal and $\{1\bar{2}12\}$ pyramidal planes and twinning in zinc.

INTRODUCTION

Chemical etching to reveal dislocations in crystals has been recognized by many investigators as a valuable tool for the study of dislocation configurations and interactions. Some aspects of the dynamic motion of dislocations have been investigated by means of this technique. Johnston and Gilman (1)* have demonstrated that a wide range of dislocation velocities may be determined by observation of etch figures before and after the application of stress to lithium fluoride crystals. An etching technique that will make possible a determination of dislocation velocities in zinc single crystals is needed for a study of the dynamic motion of dislocations in zinc.

Several reports have been made of etching procedures that reveal etch pits in zinc single crystals containing relatively high concentrations of various solute impurities such as cadmium (2), iron (3), and tin (4). Techniques that rely on the presence of impurities precipitated on dislocations usually present several distinct disadvantages. First, the mechanics of dislocation motion are changed when impurities are present because of interactions between dislocations and impurity atoms; and second, an aging treatment must follow any experiments in order to allow bulk diffusion of the impurities to dislocations. Aging treatments following deformation are undesirable in zinc because the dislocation configuration can change appreciably during the aging. Hence, a technique is desired that does not require bulk doping and that will permit observation of dislocation configurations immediately after deformation takes place.

Etching procedures that do not rely on the presence of impurities in the crystal have been developed for a number of different materials. Etch pits at dislocation sites are produced by these procedures on surfaces that are within a few degrees of a low index crystal plane, and the pits exhibit a symmetry associated with that of the crystal lattice. The mechanism of this type of etch pit formation has been discussed by

---

*One or two digit numbers appearing in parentheses refer to the references listed at the end of this report.

Riessler (5). Meleka has reported an etching procedure for zinc that produces such pits immediately after deformation (6). The density of pits produced by this technique is relatively low even after the crystals are severely deformed, so it is clear that the etchant does not reveal all of the dislocations produced by the deformation.

George (7), and Rosenbaum (8) have reported techniques for revealing dislocations on (0001) faces of high purity zinc. Dislocations that lie on the (0001) basal planes cannot be revealed by these techniques. Fig. 1 illustrates several crystallographic planes and directions in the zinc structure. Sinha and Beck (9) have recently reported a technique for revealing dislocations on $\{10\bar{1}0\}$ surfaces of zinc. This technique did not produce etch figures at dislocations in the high purity crystals used in the present study. The difference in etching behavior may be attributed to differences in the impurities in the crystals or the composition of the chemical reagents used by Sinha.

In view of the fact that a technique for revealing basal dislocations in high purity zinc without the addition of impurities to the bulk material was not available, an experimental study of chemical etching was made.

EXPERIMENTAL TECHNIQUES

Specimen Preparation

Zinc of 99.999 per cent purity obtained from the New Jersey Zinc Co. was further purified by zone refining. The refining was done in a helium atmosphere. Two separate molten zones were passed along a charge six feet in length at the rate of 2 in./hr. A total of twenty single zones were passed through the charge. The zinc in the first one third of the total charge length was used for growth of the crystals designated as zone refined.

Single crystals of both 99.999 per cent purity and zone refined zinc were grown by the Czochralski (10) and Bridgeman (11) techniques. Material grown by the Bridgeman technique was cast in graphite coated molds of pyrex.

Specimens were prepared by acid sawing the as-grown crystals with 8N nitric acid on stainless steel wire, and by cleaving on (0001) planes after the crystals had been slowly cooled to the temperatures of liquid

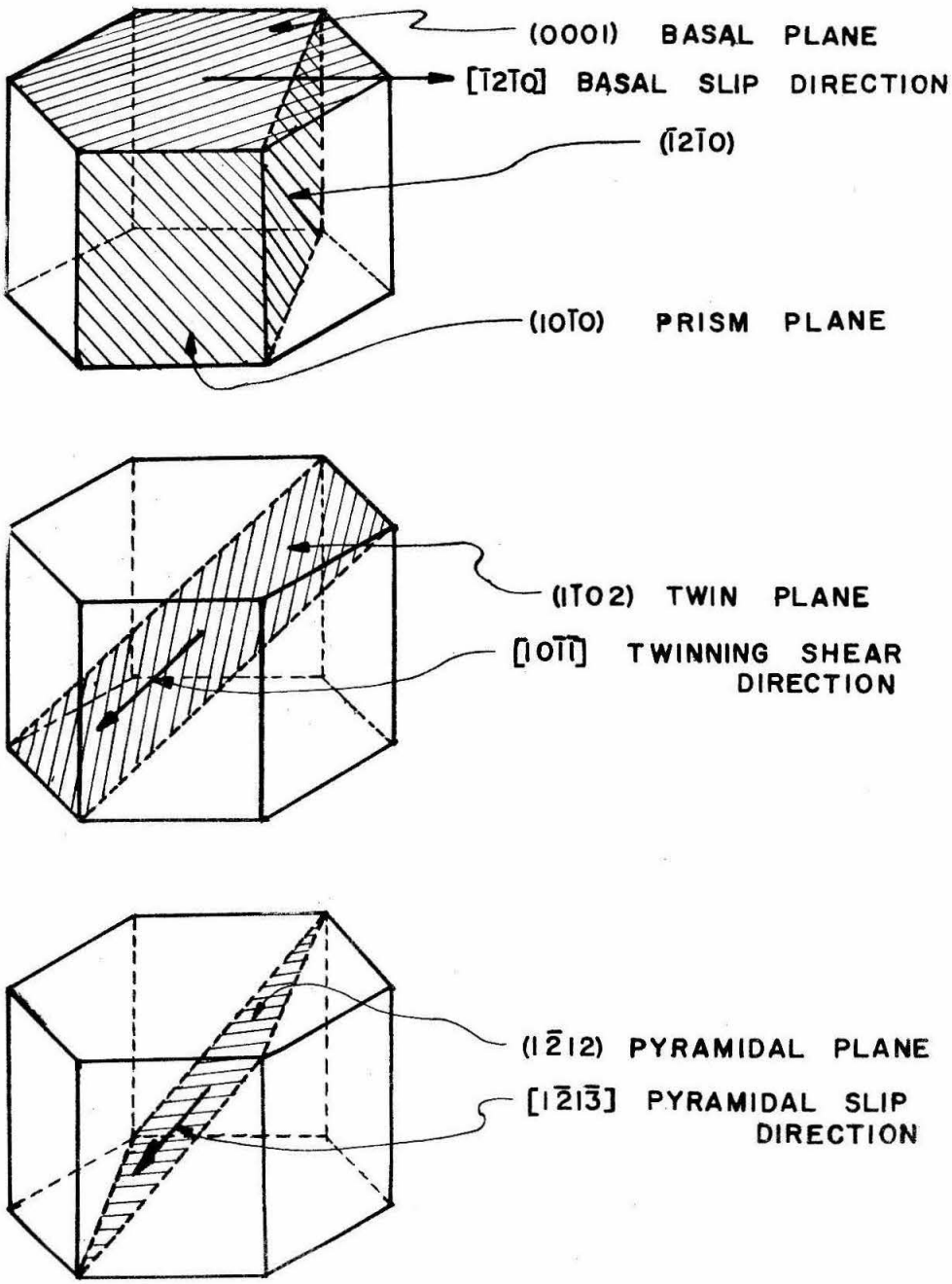

Fig. 1 Several Crystallographic Planes and Directions in Zinc Crystals.

nitrogen. The acid sawed surfaces were chemically lapped flat on a slowly turning lucite disc covered with a thin film of 8N nitric acid.

Polishing and Etching

Etch figures were produced with the four solutions listed below:

P-1 160g CrO_3
20g Na_2SO_4
500ml distilled water

P-2 Equal parts of: Methanol
30 per cent H_2O_2
conc. HNO_3

P-3 160g CrO_3
500ml distilled water

E One part: 1g $Hg(NO_3)_2$
1ml conc. HNO_3
500ml H_2O

Two parts: distilled water

The crystals were polished by dipping in solution P-1 for 20 to 100 sec with mild agitation. The crystals were occasionally dipped in solution P-2 to accelerate the polishing process. This solution removes the CrO_3 film that builds up on the surface. The last step in the polishing procedure consisted of dipping the crystals in solution P-2 to remove the CrO_3 film. Relatively rapid corrosion of crystals was noted when the CrO_3 film was not removed. After polishing, the crystals were rinsed in distilled water and dried in an air blast.

The etching procedure follows the steps listed below:

1. Dip with mild agitation in solution E, 5-6 sec.
2. Dip with mild agitation in solution P-1, 5-6 sec.
3. Dip with mild agitation in solution P-3, 2-3 sec.
4. Rinse in running tap water.
5. Rinse in running distilled water.
6. Dry in an air blast.

Best results are obtained when the polishing procedure is immediately followed by the etching procedure. A typical example of the result obtained on a $(10\bar{1}0)$ crystal face is illustrated in Fig. 2.

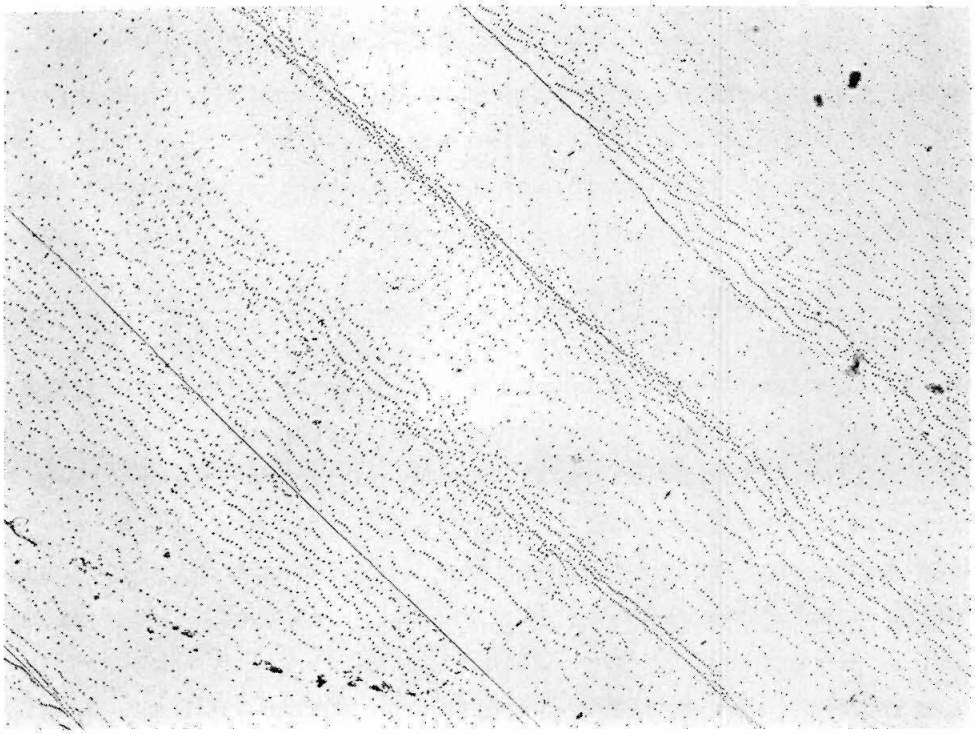

Fig. 2 Etch Figures Revealed on a (10$\bar{1}$0) prism Plane - 100X.

CORRESPONDENCE BETWEEN ETCH FIGURES AND DISLOCATIONS

As the usefulness of this etching procedure depends upon its ability to reveal dislocations, several questions must be answered. First, do all the etch patterns produced correspond to dislocations; and second, are all of the dislocations revealed? In answer to the first question, several qualitative observations of etch patterns were made to see if all of the etch figures observed could be attributed to dislocations.

Several quantitative tests were made in order to check theoretical predictions of the dislocation configurations. The etch figures examined were produced on $\{10\bar{1}0\}$ prism planes. Details which relate to the formation of the etch figures will be deferred to the next section.

Qualitative Observations illustrating that Etch Figures are Associated with Dislocations

Several specimens were observed after etching and again after repolishing and re-etching to determine the reproducibility of the etch markings with depth in the crystal. The repolishing removed from 100 to 200 microns of the surface. Fig. 3 shows etch figures which were reproduced in depth. If the figures are associated with individual dislocations which intersect the surface at right angles, the figures should repeat in depth. If the dislocations intersect the surface at an angle, the etch pattern would be expected to change, but the density of figures should not change except when dislocation nodes are removed. The reproducibility of etch figures with depth in the crystal follows the pattern expected if each figure is associated with a dislocation.

The etch patterns produced on $\{10\bar{1}0\}$ prism faces of some crystals that were etched a few minutes after deformation showed multiple figures as illustrated in Fig. 4. If the dislocations had moved during the etching process, the multiple figures could be associated with the temporary location and the final location of the dislocations. Under this assumption the larger figures as seen in Fig. 4 would correspond to the position of stationary dislocations. Occasionally streaks have been observed rather than individual figures. These could result from a relatively continuous movement of the dislocations during the etching process, or could indicate dislocations that intersect the surface at very small angles.

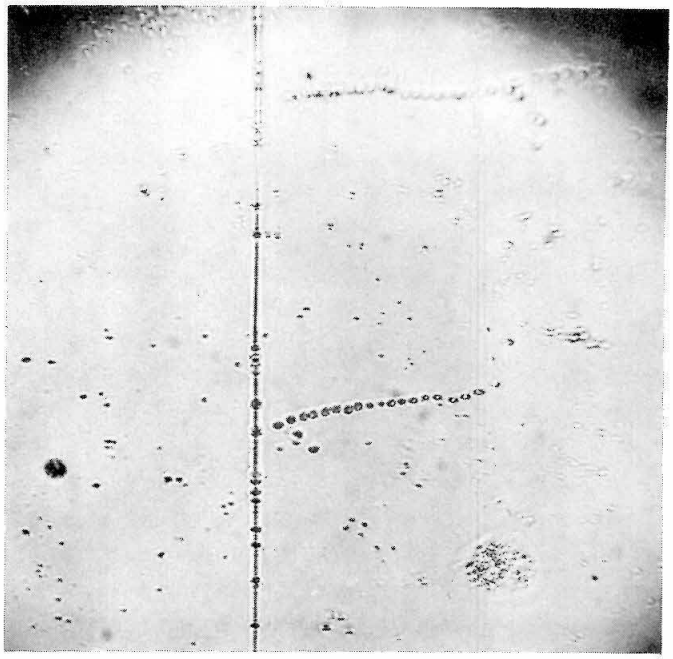

a. Initial Pattern

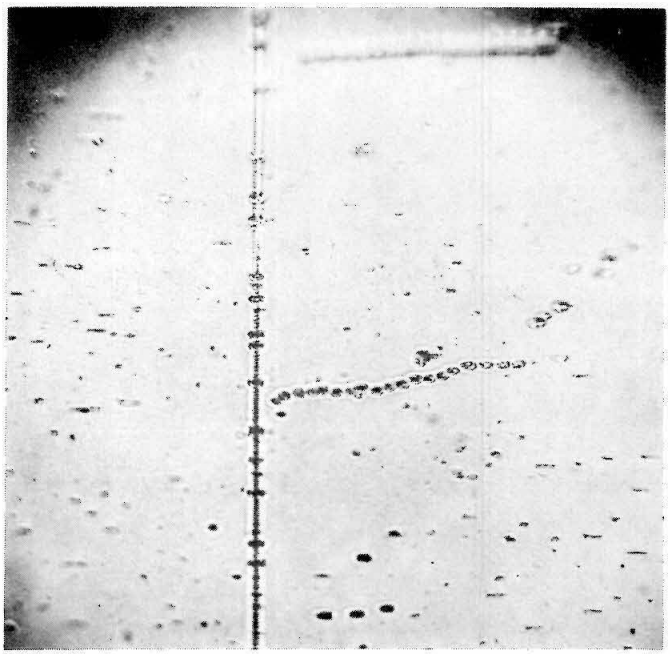

b. After Polish and Re-Etch

Fig. 3 Etch Pattern Reproduced in Depth - 500X.

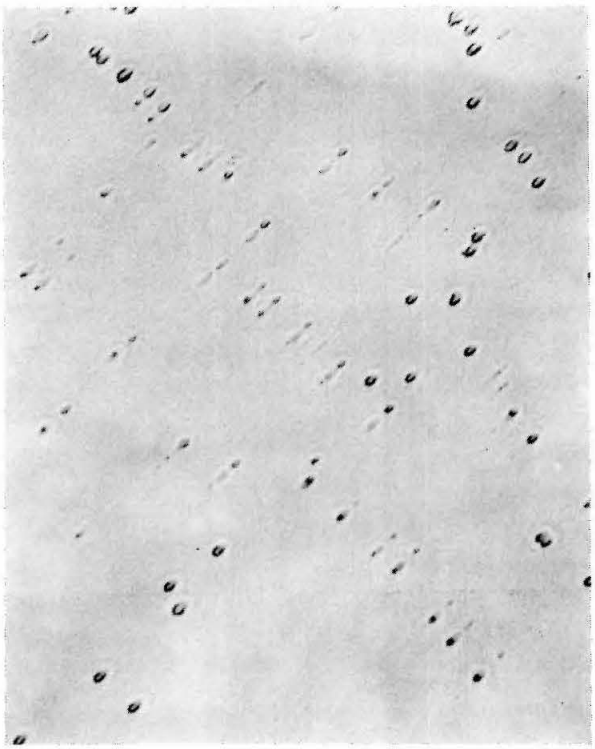

$(10\bar{1}0)$ $[\bar{1}2\bar{1}0]$

Fig. 4 Multiple Etch Figures - 500 X.

Complex pip patterns are observed on a crystal surface in the regions where local deformation has occurred. Such a pattern is shown in Fig. 5 where the local deformation was produced by striking the surface with a diamond phonograph stylus.

Etch figures are redistributed when deformed crystals are annealed. Sub-boundaries are revealed by the etchant, and the density of figures between sub-boundaries is reduced by annealing. Examples of partially polygonized structures are shown in Fig. 2 and 6.

Specific Tests for a One to One Correspondence

The density of etch figures produced by bending crystals about the $[10\bar{1}0]$ direction was determined. Three 99.999 per cent purity crystals were bent to a radius of 7.5 cm. The Nye formula predicts that a dislocation density, $\rho = (rb)^{-1}$, produces a radius of curvature r where b is the Burgers vector and the dislocations are all of the same sign and of the same slip system. If it is assumed that only basal dislocations of one sign are produced by the bending experiments, the density of dislocations corresponding to a radius of 7.5 cm in zinc is $51 \times 10^5 cm^{-2}$. The average density of figures observed in the test crystals in excess of initial density was $54 \pm 10 \times 10^5 cm^{-2}$. The results agree with the Nye calculation within the limits of experimental uncertainty.

Linear arrays of etch figures are observed that lie perpendicular to the basal planes. If these figures correspond to individual edge dislocations, the array represents a tilt boundary of angle $\theta = \frac{b}{h}$ where h is the spacing of the figures. The angle of a tilt boundary in a zone refined crystal was measured by means of an interference microscope on a cleaved (0001) basal plane with a light source of 2675Å wave length. The interference measurement gave $\theta = 1.9 \pm 0.2 \times 10^{-4}$ radians. The separation of figures was measured on a $(10\bar{1}0)$ plane adjacent to the cleaved surface. The angle calculated from the figure spacing, taking $b = 2.66$Å (lattice parameter in the $[\bar{1}2\bar{1}0]$ direction), gave $\theta = 1.82 \pm 0.04 \times 10^{-4}$ radians. These values agree within the limits of experimental error. The figures must therefore correspond to individual edge dislocations.

Hexagonal networks of screw dislocations that lie on basal planes in

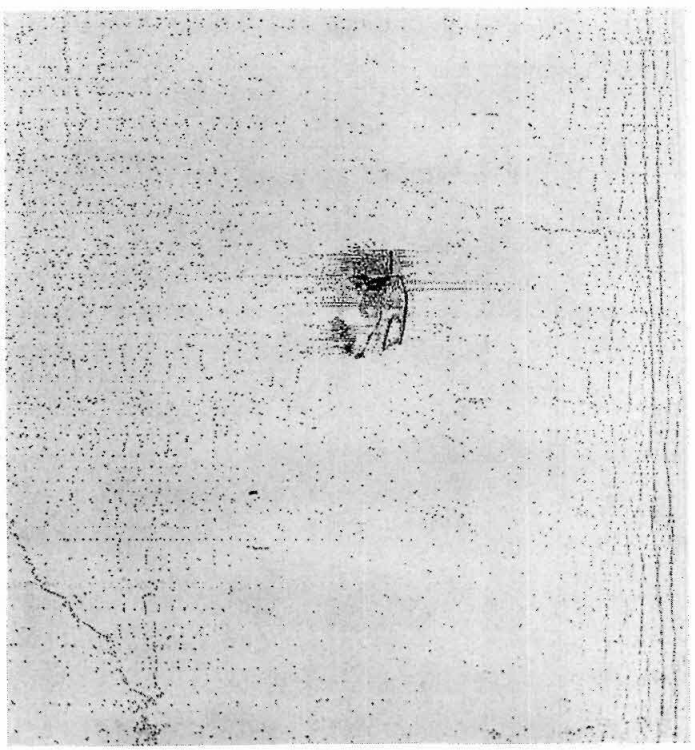

$(10\bar{1}0)$ $[\bar{1}2\bar{1}0]$

Fig. 5 Etch Figures Resulting from Surface Deformation - 100X.

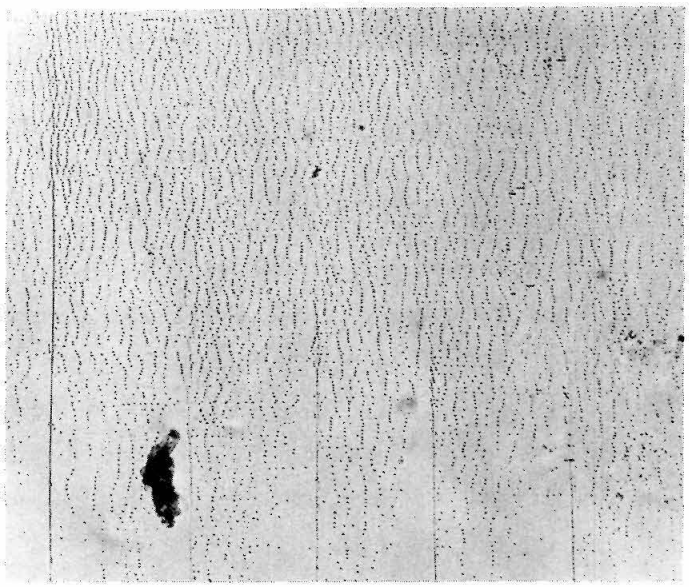

$(10\bar{1}0)$ $[\bar{1}2\bar{1}0]$

Fig. 6 Partially Polygonized Structure - 100 X.

zinc have been observed by Berghezan et al by transmission electron microscopy (12). These networks result from twist about a [0001] axis of the crystal (13). If the networks are composed of screw dislocations of length s, as shown in Fig. 7, and the networks are equally spaced with a density of z per unit length along the [0001] axis, the twist per unit length is $\theta = zb/\sqrt{3}s$. The density of screw dislocations intersecting the $(10\bar{1}0)$ plane is then $2\theta/\sqrt{3}b$.

A crystal of 99.999 per cent purity was twisted about its [0001] axis and the twist was measured to be 0.42 ± 0.02 radians per cm. The figures on a $(10\bar{1}0)$ surface of this crystal are shown in Fig. 8, and their density was determined to be 19 ± 3 x $10^6 cm^{-2}$. The density calculated from the above formula with the measured values of twist and b for a complete basal dislocation is 18.2 ± .9 x $10^6 cm^{-2}$. The difference between the observed and calculated densities should represent the initial dislocation density. The initial density was not determined, but similar crystals have background densities that range from 0.4 x 10^5 to 20 x $10^5 cm^{-2}$. The density of figures in the twisted crystal therefore corresponds, within the limits of experimental error, to the density of screw dislocations predicted by the model.

While the experimental evidence presented above does not prove that all dislocations intersecting $\{10\bar{1}0\}$ surfaces are revealed by the etching procedure, it indicates strongly that all edge and screw dislocations that lie on (0001) planes are revealed, and that each etch figure represents the intersection of a dislocation with the surface. Qualitative observations presented in a subsequent section indicate that non-basal dislocations are also revealed on prism surfaces.

FORMATION OF ETCH FIGURES

Several experiments were made to investigate the etching on different crystallographic surfaces, and to determine the effect of the mercury introduced by solution E in the etching procedure. The following observations were made.

1. At the sites of dislocation-surface intersections on $\{10\bar{1}0\}$ surfaces, small hillocks or pips are formed rather than etch pits. This

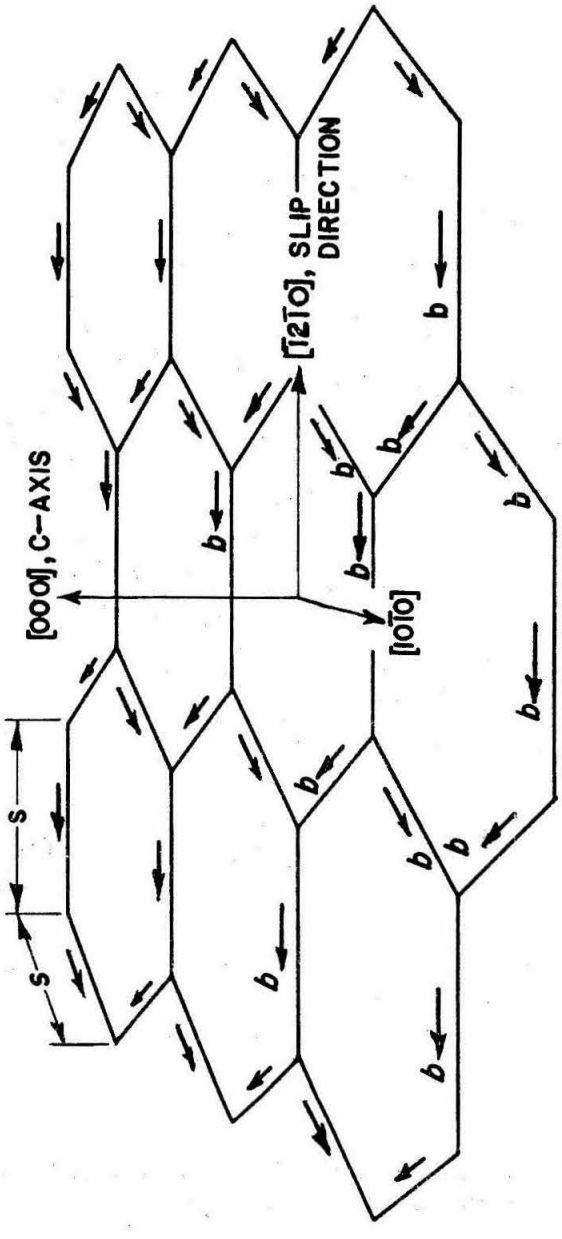

Fig. 7 Hexagonal Screw Dislocation Model

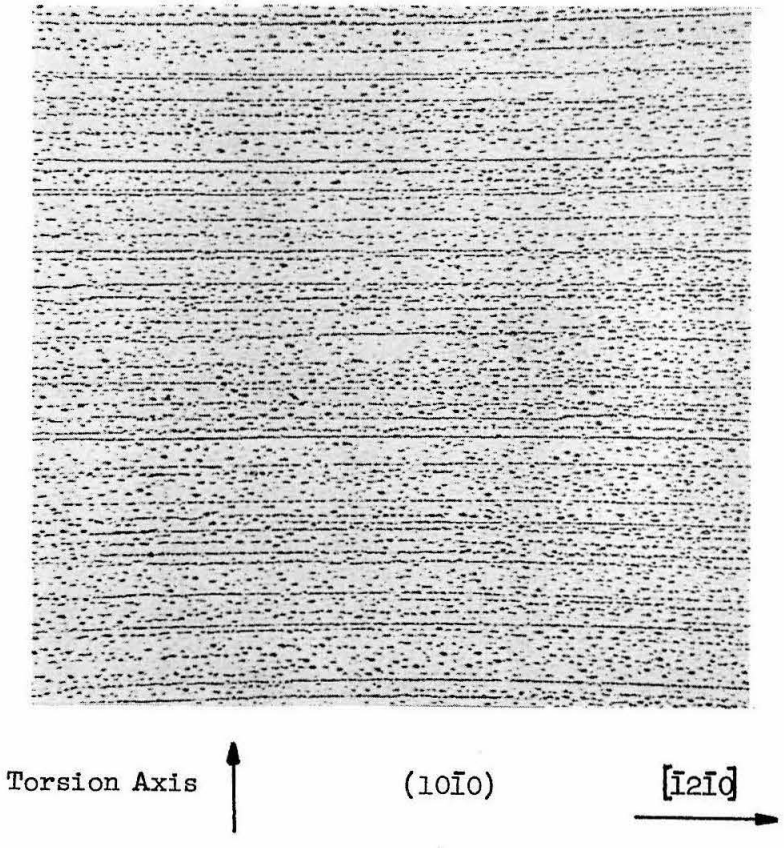

Fig. 8 Etch Figures Resulting from Torsional Deformation about an [0001] Axis - 500X.

was determined by microscopic examination with side illumination of the specimen.

2. The fine focus scale on a microscope was used to determine the amount of material removed by a 100 sec polish. The rate of removal with the P-1 solution alone is 0.19 microns/sec. With intermittent rinses in the P-2 solution, the rate is about 0.25 microns/sec. The rate of polishing on prism faces is essentially independent of the presence of mercury.

3. Observation of the etching behavior on crystals that were twisted about the [0001] axis permits a determination of the effect of crystal orientation on a single, plane observation surface. Etching is sensitive to the crystallographic orientation of crystal surfaces that are perpendicular to the (0001) basal plane, while polishing with solutions P-1 and P-2 is not. Good etch figures can be obtained on surfaces oriented within 5° of the $\{10\bar{1}0\}$ prism plane. Etch pips have been observed on surfaces at angles as great as 15° from the prism plane. Fig. 9a shows a region of the surface which is a prism plane of the twisted crystal. Fig. 9b shows a region of the surface which is oriented approximately 5.5° from the prism plane of the twisted crystal. A lower density of pips is observed in Fig. 9b, and the etched surface of the specimen is not as smooth as that in Fig. 9a.

4. In specimens that have previously been etched, new etch pips will form at areas of new deformation upon immersion in the polishing solutions P-1 and P-3. This will occur even if the mercury was introduced several weeks previous to the deformation.

5. A specimen was bent while it was in solution P-1 during step 3 of the etching procedure. The succeeding steps of the etching were then taken as usual. Examination of the surface showed a pip density considerably in excess of the initial density. The majority of the pips could be associated only with dislocations formed during the deformation.

6. Larger pips are formed when the specimen is immersed for longer periods in solution E.

7. Repolishing after etching is greatly facilitated by placing the specimens along with an indium getter in a 10^{-6} mm Hg vacuum for 12 hr or more. After the vacuum treatment, a good polish can be obtained by

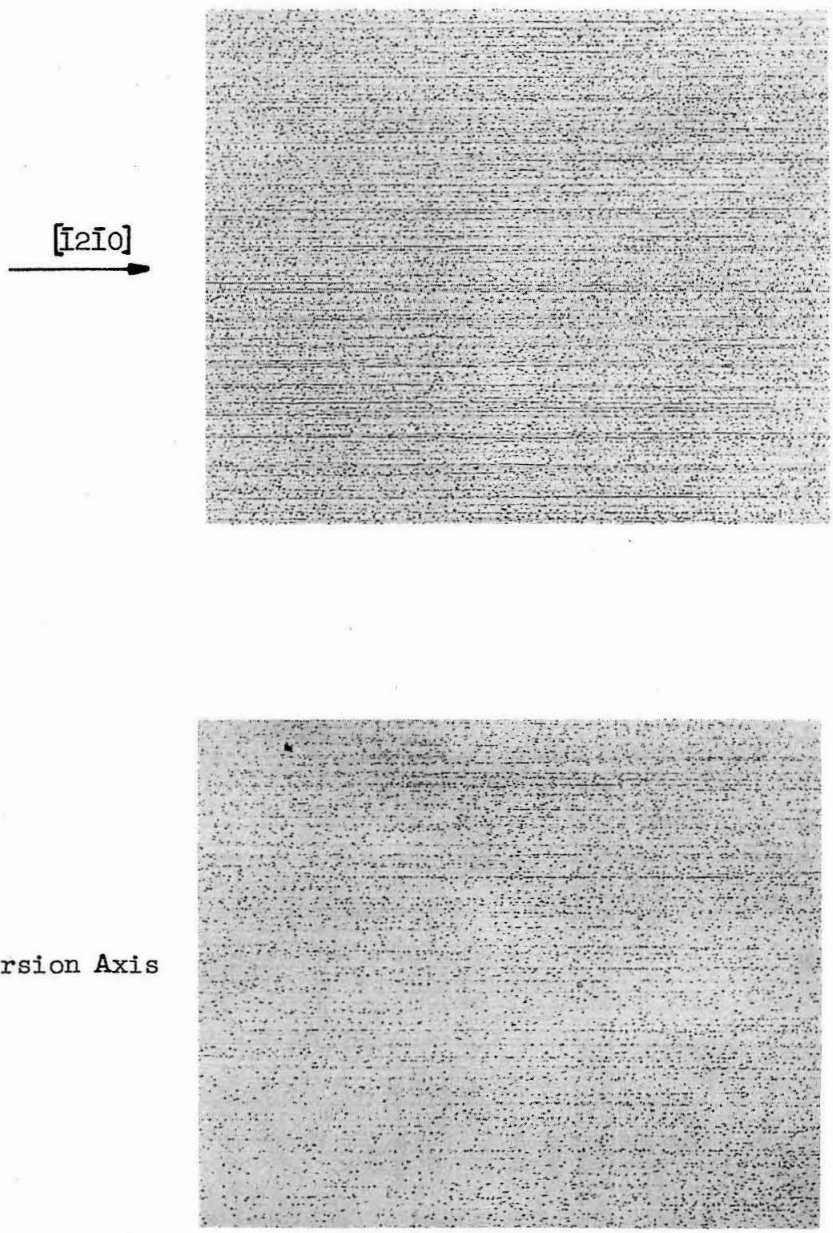

b. 5.5° From a Prism Plane

Fig. 9 Variation of Etch Figure Densities with Prism Plane Orientation. Twisted Specimen - 150X.

removing as little as 50 microns of the crystal surface. Without the vacuum treatment, several thousand microns must be removed to obtain a good polish.

A tentative explanation of the formation of etch figures on prism surfaces may be made if it is assumed that the mercury introduced by solution E rapidly diffuses over the polished surface and concentrates at dislocation sites. The formation of pips rather than pits at dislocations which intersect prism surfaces may then be attributed to the relatively high concentration of mercury at these sites if the mercury retards the rate of polishing.

The observations indicate that surface diffusion of the mercury occurs at a very high rate compared to bulk diffusion. The concentration of mercury on a crystal surface is sufficiently large, after two weeks aging at room temperature, that surface diffusion of mercury to newly formed dislocations takes place and pips are formed on polishing immediately after deformation.

Additional experiments are being conducted in an attempt to shed light on the mechanism of the formation of etch figures, and the orientation dependence of the etching.

OBSERVATIONS MADE WITH THE USE OF THE ETCHING TECHNIQUE

A. Dislocation Densities

The etching technique was used to compare the dislocation density in mold grown crystals with that in crystals pulled from the melt. The dislocation density was taken to be the pip density on a prism face of the crystal. Crystals grown in a mold by the Bridgeman technique had densities in the range 1-10 x 10^5 lines/cm^2. Crystals pulled from the melt by the Czochralski technique were seeded with mold-grown crystals and withdrawn from the melt at the rate of 1.5 in./hr. In general the dislocation density in the pulled crystals was one order of magnitude greater than that in the seed.

B. Sub-Boundaries

Examination of a number of crystals after small amounts of deformation reveals that the dislocation distribution around sub-boundaries is very

different from the distribution between sub-boundaries. The number of dislocations piled up on the boundary shown in Fig. 10 indicates that the boundary is a relatively effective obstacle to dislocation motion. This boundary may be a simple tilt boundary, or a more complex sub-boundary. Li (14) concludes from theoretical calculations that a simple tilt boundary is not a very effective barrier to the penetration of parallel dislocations of the same Burgers vector. If, however, the probability is high that a moving dislocation will meet a boundary before some other obstacle is encountered, the boundaries will act as relatively effective obstacles. This is the case in zinc crystals of high purity with low dislocation density between sub-boundaries.

C. Non-Basal Slip and Twinning

The correspondence between etch figures and non-basal dislocations was investigated in a crystal deformed by a loading procedure that minimized basal slip. A zone refined crystal was loaded in compression along the [0001] axis until twinning occurred. Deviation from a linear load-deflection curve was noted at a compressive stress of 6,020 lb/in.^{2} This could result from pyramidal slip on $\{1\bar{2}12\}$ planes in the $\langle 1\bar{2}1\bar{3}\rangle$ direction at a resolved shear stress of 600 lb/in.^{2} Such non-basal deformation has been reported by Bell and Cahn (15). Twinning occurred at a shear stress of 3,000 lb/in.^{2}, resolved in the $\{1\bar{1}02\}$ twinning plane. Fig. 11 illustrates twin traces on $(10\bar{1}0)$, (0001) and $(\bar{1}2\bar{1}0)$ planes of the un-etched specimen. The twin traces are consistent with the well-known $\{1\bar{1}02\}$ twinning planes.

The $(10\bar{1}0)$ prism plane of the compression specimen was etched to observe the pip arrays associated with twins. Etching of twinned material produced a rough finish due to the fact that the surface was mis-oriented from a $\{10\bar{1}0\}$ plane. Fig. 12 illustrates the appearance of twinned and untwinned material and several pip arrays associated with the tips of twins. Fig. 12a is a $(10\bar{1}0)$ surface of the compression specimen and Fig. 12b is a $(10\bar{1}0)$ surface of a specimen of similar initial dislocation density which was accidentally damaged. The large increase in background density in the compressed specimen is the result of non-basal slip before twinning. Pips lined up parallel to the twin tips and tilt boundaries

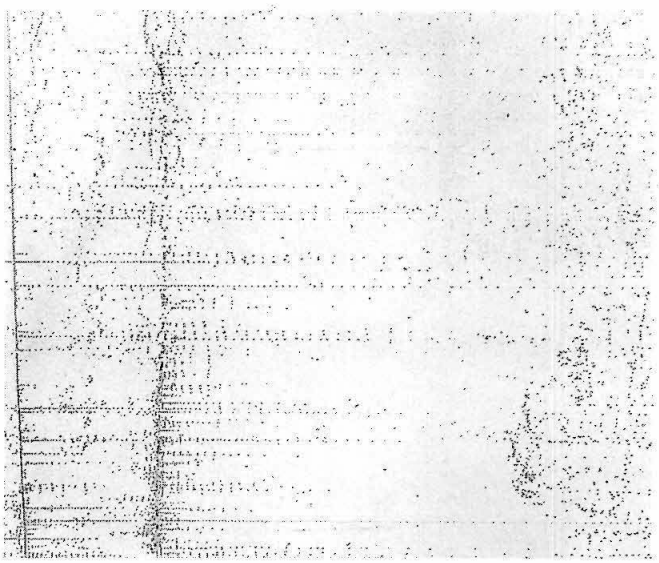

Fig. 10 Dislocations Piled up on Sub-Boundary - 100X.

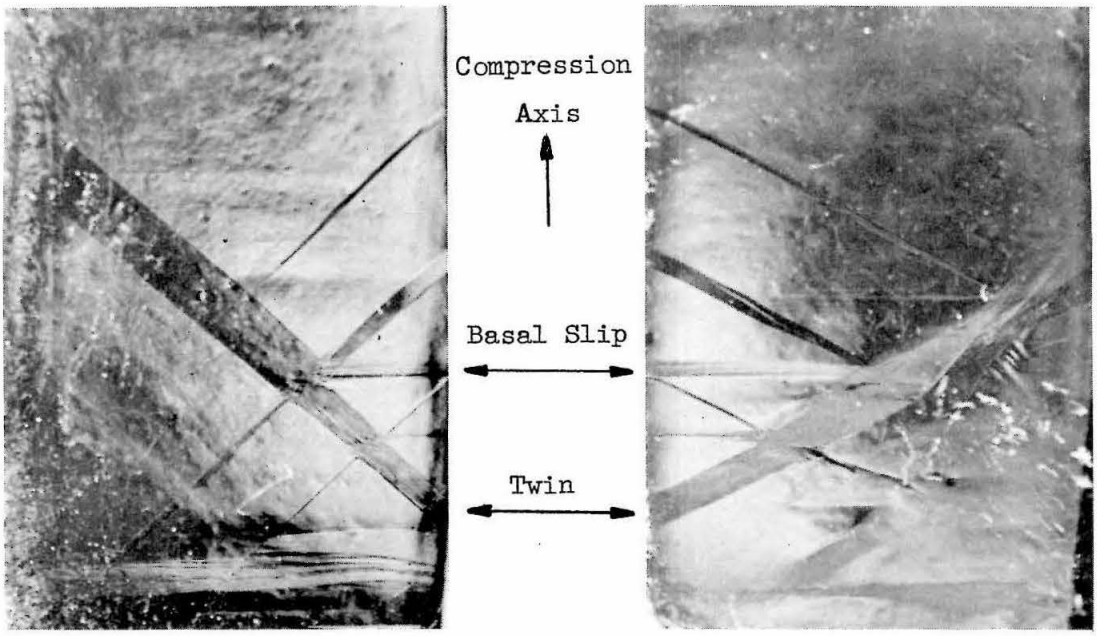

a. $(10\bar{1}0)$ of Untwinned Material

b. $(\bar{1}2\bar{1}0)$ of Untwinned Material

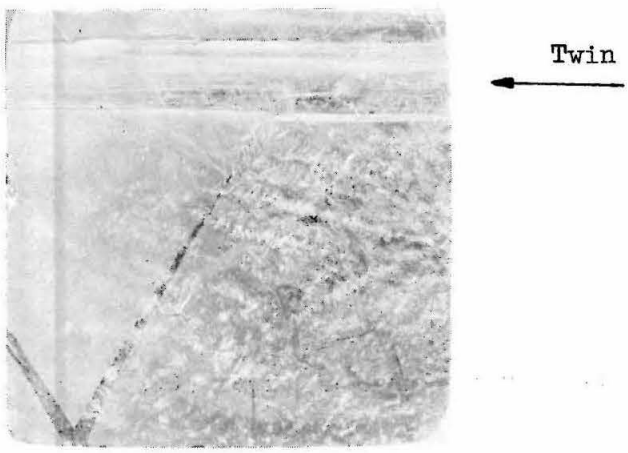

c. (0001) of Untwinned Material

Fig. 11 Unetched Compression Specimen - 7X.

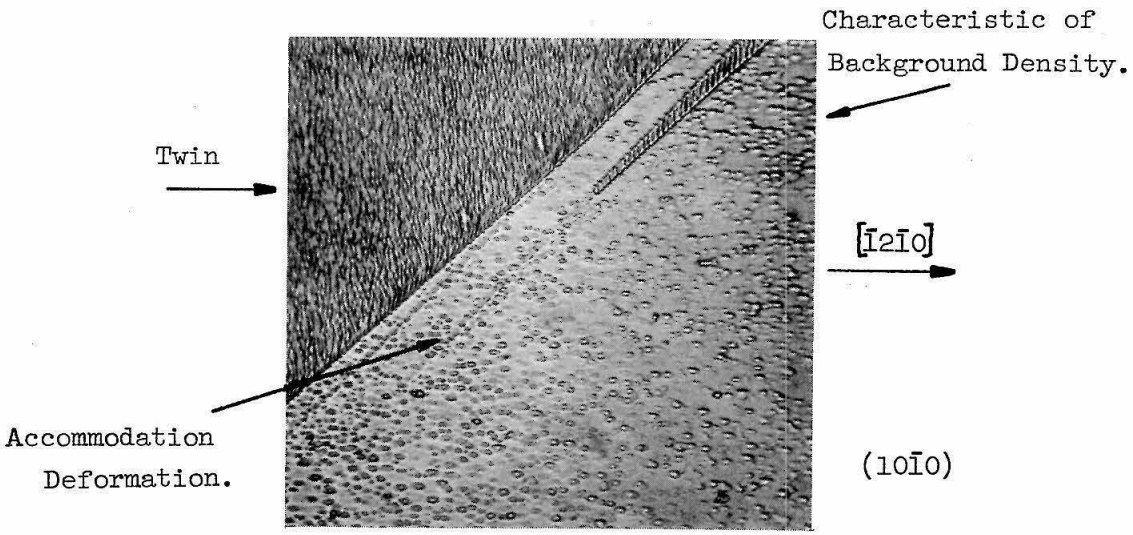

a. Compression Specimen - 750X.

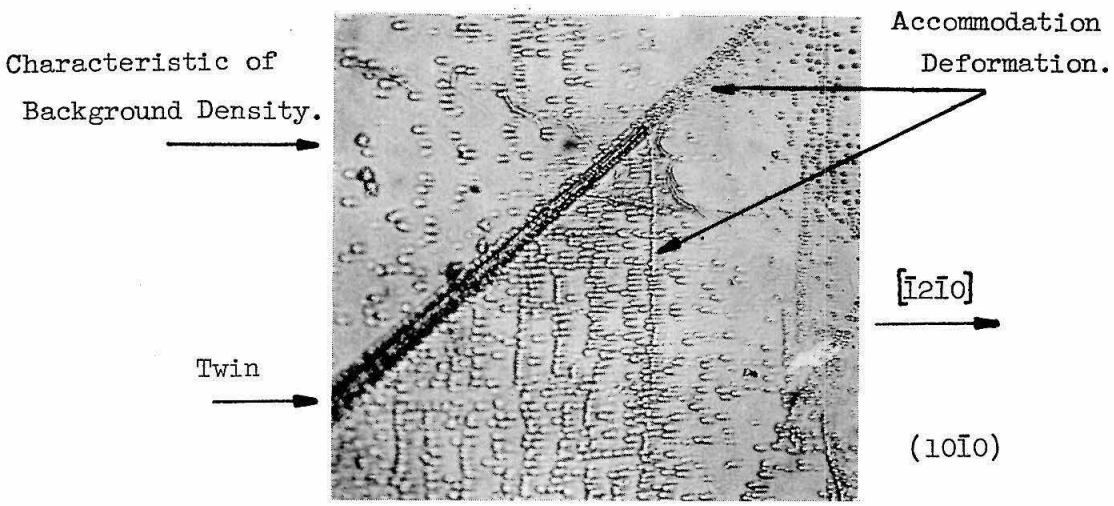

b. Accidental Damage - 500X.

Fig. 12 Etch Figures Associated with Twin Tips.

eminating from tips represent accommodation deformation as explained by Rosenbaum (8). The slip lines corresponding to (0001) basal slip as seen in Fig. 11 result from similar accommodation to the high stress regions at twin intersections.

To study the deformation within twinned material, a $(10\bar{1}0)$ prism face was exposed by sectioning the compression specimen with an acid saw almost parallel to the (0001) basal plane of the untwinned material. The surfaces of the twinned material, as seen in Fig. 11c, are within 0.1° of the $\{10\bar{1}0\}$ prism planes of twinned material. The specimen was sectioned in order to examine regions that were not affected by slight inhomogeneities in the load applied to the ends of the specimen. Fig. 13 shows pip patterns as revealed on a $(10\bar{1}0)$ face of twinned material. Pips labeled P can be observed running parallel to the $(1\bar{2}12)$ slip plane trace which may indicate that the pips correspond to pyramidal slip dislocations. The pip arrays in Fig. 12 and 13 only occur in short segments and are not restricted to narrow bands. This results from the fact that there are six intersecting $\{1\bar{2}12\}$ type planes each with the same resolved shear stress. Interaction of the dislocations on different intersecting slip planes prevents the formation of slip bands such as those observed on the basal planes. This also explains the absence of $\{1\bar{2}12\}$ pyramidal slip lines on the specimen surface in Fig. 11.

An attempt was made to etch a (0001) basal plane of both the twinned and untwinned regions of the deformed crystal. There is some doubt as to whether all dislocations threading the basal plane are revealed by the etching procedure. Rosenbaum's etch may be more suitable on (0001) planes. Fig. 14 illustrates several arrays that were revealed on planes misoriented from the (0001) basal plane by 4.1°. Pips lined up at 30° to the $\langle\bar{1}2\bar{1}0\rangle$ slip direction in both the twinned and untwinned material provides further confirmation of the existence of $\{1\bar{2}12\}$ pyramidal slip. In this case the pips probably correspond to screw dislocations lying along the $[1\bar{2}1\bar{3}]$ direction in the $(1\bar{2}12)$ plane. Fig. 15 illustrates an array that was revealed on the basal plane of untwinned material. Pips lined up parallel to the $[\bar{1}2\bar{1}0]$ direction may indicate $\langle 10\bar{1}\bar{1}\rangle$ screw dislocations in a $\{1\bar{1}02\}$ twinning plane. This type of array has been observed by Rosenbaum (8).

An interesting example of dislocations on intersecting non-basal slip planes, as revealed on a $(10\bar{1}0)$ surface, is shown in Fig. 16. The specimen was damaged by intentionally striking it on a corner with a glass plate. Pip lines labeled P probably correspond to dislocations in a $(2\bar{1}\bar{1}2)$ plane. Lines labeled Q could correspond to dislocations in the $(1\bar{2}12)$ plane or the $(1\bar{1}02)$ twinning plane.

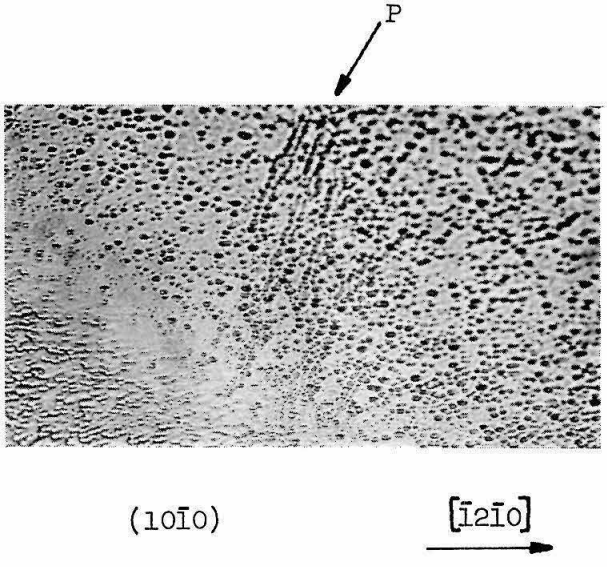

Fig. 13 Etch Figures in Twinned Material of Compression Specimen - 500X.

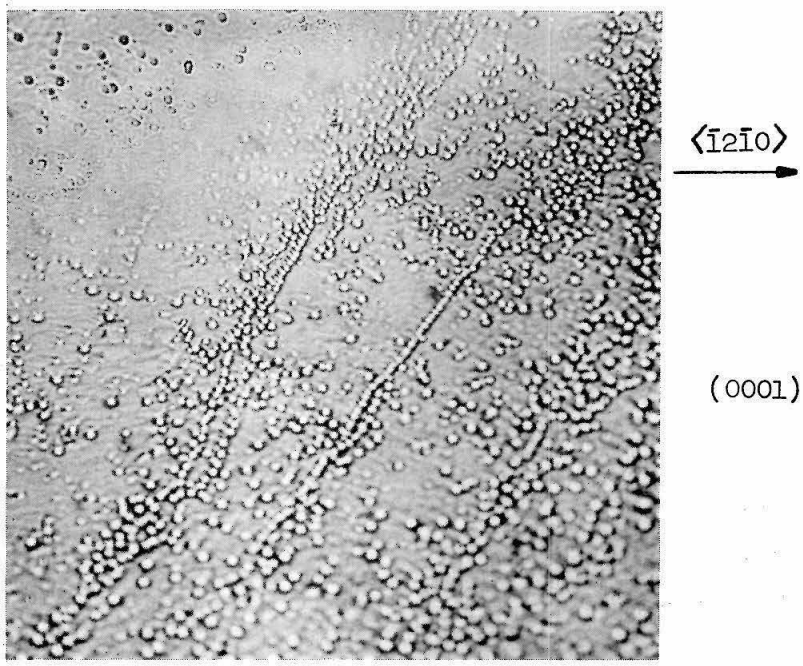

a. Untwinned Material - 500X.

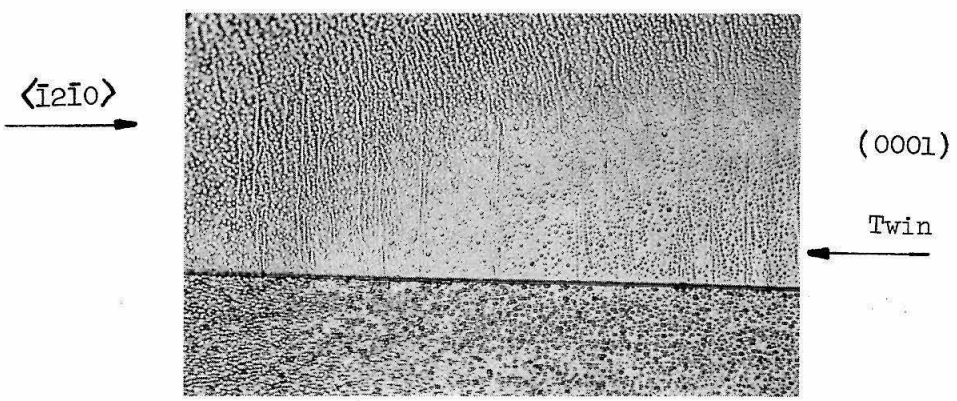

b. Twinned Material - 250X.

Fig. 14 Etch Figures Revealed on (0001) Basal Planes of Compression Specimen.

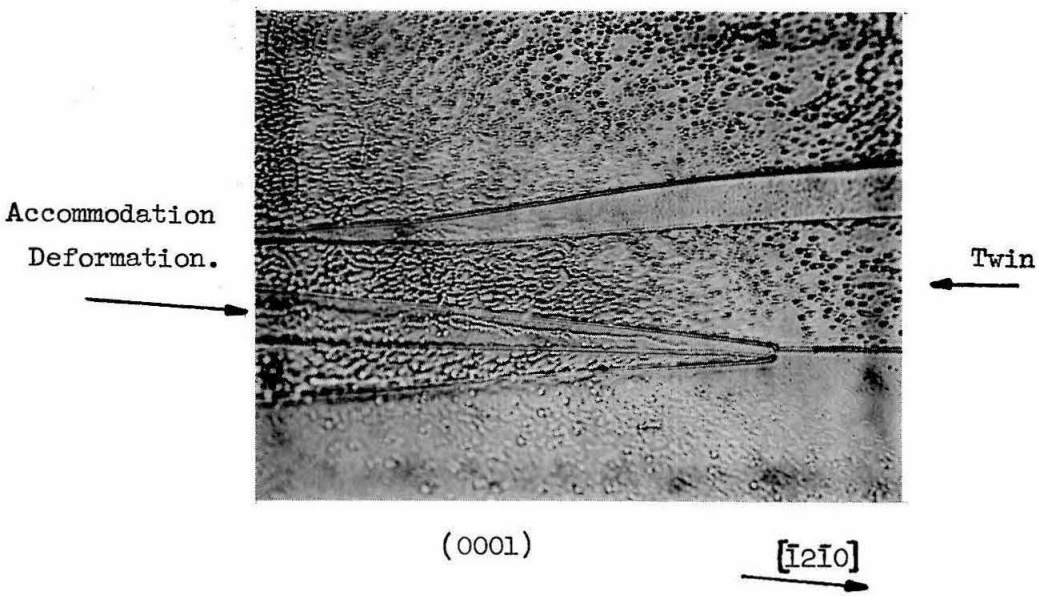

Fig. 15 Etch Figures on Basal Plane of Untwinned Material - 500X.

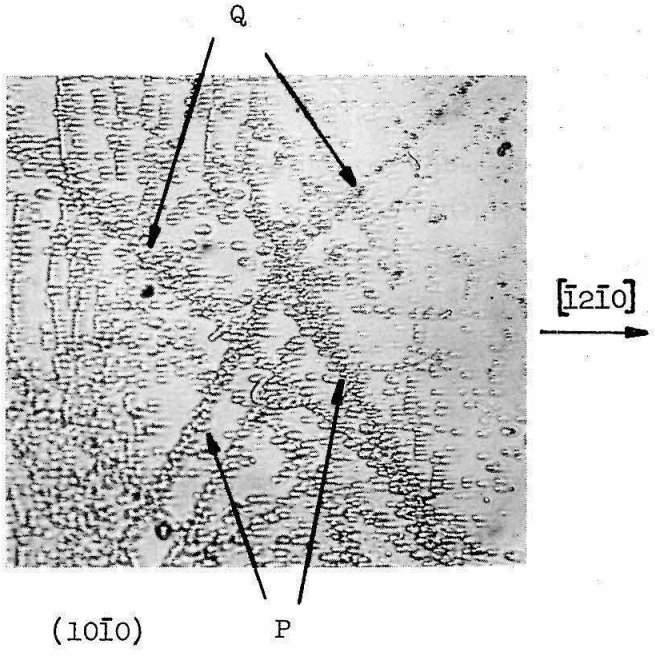

Fig. 16 Non-Basal Dislocations Revealed on a (10$\bar{1}$0) Prism Plane - 500X.

SUMMARY AND CONCLUSIONS

The etching procedure described in this report has been shown to reveal basal and non-basal dislocations on $\{10\bar{1}0\}$ prism planes in high purity zinc. Etch figures at dislocation sites are also produced on (0001) basal planes.

The mercury that is introduced to the specimen surface in the etching procedure is believed to concentrate at dislocations which intersect prism surfaces. Pips rather than pits are then produced at dislocation sites when the specimen is subsequently polished. The mercury may be removed from the surface of the specimen by vacuum distillation followed by chemical polishing.

Surface doping of high purity crystals to retard or accelerate chemical attack at dislocation sites is a useful experimental technique. Since surface diffusion rates are considerably higher than bulk diffusion rates, surface doping requires a relatively short aging time for the impurities to diffuse to dislocations. The impurity may be removed chemically or by distillation before it appreciably alters the purity of the bulk of the crystal.

ACKNOWLEDGEMENT

The authors wish to express their thanks to Professors D. S. Clark and D. S. Wood for their suggestions during the course of this work and for their comments on the manuscript.

REFERENCES

1. W. G. Johnston and J. J. Gilman, "Dislocation Velocities, Dislocation Densities, and Plastic Flow in Lithium Fluoride Crystals", Journal of Applied Physics (1959), Vol. 30, p. 129.

2. J. J. Gilman, "Etch Pits and Dislocations in Zinc Monocrystals", Transactions of the American Institute of Mining, Metallurgical and Petroleum Engineers (1956), Vol. 206, p. 998.

3. V. M. Stepanova and A. A. Urusovskaya, "The Etch Method for Revealing Dislocations in Zinc Crystals", Soviet Physics Crystallography (1959), Vol. 4, p. 913.

4. G. Bassi and J. P. Hugo, "Etch Pits in Zinc", Journal of the Institute of Metals (1958), Vol. 87, p. 376.

5. W. Riessler, "Dislocations and the Growth of Etch Pits", Zeitschrift fur Angewandte Physik (1960), Vol. 12, p. 433.

6. A.H.A. Méléka, "Etch Pits and Dislocations in Zinc Single Crystals", Philosophical Magazine (1956), Vol. 1, Eighth Series, p. 803.

7. Joy George, "Dislocation Etch Pits in Zinc Crystals", Philosophical Magazine (1959), Vol. 4, Eighth Series, p. 1142.

8. H. S. Rosenbaum, "Non-Basal Slip and Twin Accommodation in Zinc Crystals", Acta Metallurgica (1961), Vol. 9, p. 742.

9. R. P. Sinha and P. A. Beck, "Polygonization in Bent Zinc Crystals", Journal of Applied Physics (1961), Vol. 32, p. 1222.

10. J. Czochralski, "A New Method for Measuring the Crystallization Rate of a Metal", Zeitschrift für Physikalische Chemie (1918), Vol. 92, p. 219.

11. P. W. Bridgeman, "Certain Physical Properties of Single Crystals of Tungsten, Antimony, Bismuth, Tellurium, Cadmium, Zinc, and Tin", Proceedings of the American Academy of Arts and Sciences (1925), Vol. 60, p. 305.

12. A. Berghezan, A. Fourdeux, and S. Amelinck, "Transmission Electron Microscopy Studies of Dislocations and Stacking Faults in a Hexagonal Metal: Zinc", Acta Metallurgica (1961), Vol. 9, p. 464.

13. N. Brown, "Stress Analysis of a Single Crystal in Pure Torsion", Transactions of the American Institute of Mining, Metallurgical and Petroleum Engineers (1955), Vol. 203, p. 134.

14. J.C.M. Li, "The Interaction of Parallel Edge Dislocations with a Simple Tilt Dislocation Wall", Acta Metallurgica (1960), Vol. 8, p. 296.

15. R.L. Bell and R.W. Cahn, "The Dynamics of Twinning, and the Interaction of Slip and Twinning in Zinc Crystals", Proceedings of the Royal Society of London (1957), Vol. 239 Series A, p. 494.

DISTRIBUTION LIST

Copy Number	
1 - 2	Chief of Naval Research Department of the Navy Washington 25, D.C. Attention: Code 423
3	Commanding Officer Office of Naval Research Branch Office 495 Summer Street Boston 10, Massachusetts
4	Commanding Officer Office of Naval Research Branch Office 346 Broadway New York 13, New York
5	Commanding Officer Office of Naval Research Branch Office 86 E. Randolph Street Chicago 1, Illinois
6	Commanding Officer Office of Naval Research Branch Office 1030 E. Green Street Pasadena, California
7	Commanding Officer Office of Naval Research Branch Office 1000 Geary Street San Francisco 9, California
8 - 12	Assistant Naval Attache for Research Office of Naval Research Branch Office, London Navy 100, Box 39 F.P.O., New York, N.Y.
13 - 18	Director U. S. Naval Research Laboratory Washington 25, D.C. Attn: Technical Information Officer, Code 2000
19 - 20	Chief, Bureau of Aeronautics Department of the Navy Washington 25, D.C. Attention: Code AE 4 : Code TD 41

Copy Number	Distribution List - Cont'd
21	Commanding Officer U. S. Naval Air Material Center Philadelphia, Pennsylvania Attn: Aeronautical Materials Laboratory
22 - 24	Chief, Bureau of Ordnance Department of the Navy Washington 25, D.C. Attention: Code Res-1e : Code Ad-3 : Code Rec-1
25	Superintendent U. S. Naval Gun Factory Washington 25, D.C. Attention: Code 720
26	Commanding Officer U. S. Naval Ordnance Laboratory White Oaks, Maryland
27	Commanding Officer U. S. Naval Ordnance Test Station Inyokern, California
28	Commanding Officer U. S. Naval Proving Ground Dahlgren, Virginia Attention: Laboratory Division
29 - 31	Chief, Bureau of Ships Department of the Navy Washington 25, D.C. Attention: Code 330 : Code 337L : Code 343
32	Commanding Officer U. S. Naval Engineering Experiment Station Annapolis, Maryland Attention: Metals Laboratory
33	Materials Laboratory New York Naval Shipyard Brooklyn 1, New York Attn: Code 907
34	Chief, Bureau of Yards and Docks Department of the Navy Washington 25, D.C. Attention: Research and Standards Division

Copy Number — Distribution List - Cont'd

35
Commanding Officer
David Taylor Model Basin
Washington 7, D.C.

36
Post Graduate School
U. S. Naval Academy
Monterey, California
Attn: Department of Metallurgy

37
Office of Technical Services
Department of Commerce
Washington 25, D.C.

38 - 42
Armed Services Technical Information Agency (ASTIA)
Documents Service Center
Knott Building
Dayton 2, Ohio

43 - 44
Commanding Officer
Watertown Arsenal
Watertown, Massachusetts
Attn: Ordnance Materials Research Office
: Laboratory Division

45
Commanding Officer
Frankford Arsenal
Frankford, Pennsylvania
Attn: Laboratory Division

46
Commanding Officer
Office of Ordnance Research
Box CM, Duke Station
Duke University
Durham, North Carolina
Attn: Metallurgy Division

47 - 49
Commander
Wright Air Development Center
Wright-Patterson Air Force Base, Dayton, Ohio
Attn: Aeronautical Research Lab. (WCRRH)
: Aeronautical Research Lab. (WCRRL)
: Materials Laboratory (WCRTL)

50
U. S. Air Force ARDC
Office of Scientific Research
Washington 25, D.C.
Attn: Solid State Division (SRQB)

51 - 52
National Bureau of Standards
Washington 25, D.C.
Attn: Metallurgy Division
: Mineral Products Division

Copy Number	Distribution List - Cont'd
53	National Advisory Committee for Aeronautics 1512 H Street, N.W. Washington 25, D.C.
54	National Advisory Committee for Aeronautics Lewis Flight Propulsion Laboratory Cleveland, Ohio Attn: Materials and Thermodynamics Division
55	U. S. Atomic Energy Commission 1901 Constitution Avenue Washington 25, D.C. Attn: Technical Library
56 - 57	U. S. Atomic Energy Commission Washington 25, D.C. Attn: Metals and Materials Branch Division of Research : Eng. Development Branch Division of Reactor Development
58	Argonne National Laboratory P. O. Box 299 Lemont, Illinois Attn: H. D. Young, Librarian
59	Brookhaven National Laboratory Technical Information Division Upton, Long Island, New York Att: Research Library
60	Union Carbide Nuclear Co. Oak Ridge National Laboratory P. O. Box P Oak Ridge, Tennessee Attn: Laboratory Records Department
61	Los Alamos Scientific Laboratory P. O. Box 1663 Los Alamos, New Mexico Attn: Report Librarian
62	Union Carbide Nuclear Co. K-25 Plant Records Department P. O. Box P Oak Ridge, Tennessee
63	Union Carbide Nuclear Co. Y-12 Plant Records Department Central Files P. O. Box Y Oak Ridge, Tennessee

Copy Number	Distribution List - Cont'd
64	General Electric Company P. O. Box 100 Richland, Washington Attn: Technical Information Division
65	Iowa State College P. O. Box 14A, Station A Ames, Iowa Att: F. H. Spedding
66	Knolls Atomic Power Laboratory P. O. Box 1072 Schenectady, New York Attn: Document Librarian
67	Mound Laboratory Monsanto Chemical Co. P. O. Box 32 Miamisburg, Ohio
68	U. S. Atomic Energy Commission New York Operations Office 70 Columbus Avenue New York 23, New York Attn: Document Custodian
69	Sandia Corporation Sandia Base Albuquerque, New Mexico Att: Library
70	U. S. Atomic Energy Commission Technical Information Service Extension P. O. Box 62 Oak Ridge, Tennessee Attn: Reference Branch
71	University of California Radiation Laboratory Information Division Room 128, Building 50 Berkeley, California Attn: R. K. Wakerling
72	Bettis Plant U. S. Atomic Energy Commission Bettis Field P. O. Box 1468 Pittsburgh 30, Pennsylvania Attn: Mrs. Virginia Sternberg, Librarian
73	Officer in Charge U. S. Naval Civil Engineering Research and Evaluation Laboratory Construction Battalion Center Port Hueneme, California

Copy Number — Distribution List - Cont'd

74
Professor E. R. Parker
Division of Mineral Technology
University of California
Berkeley 4, California

75
Professor A. R. Troiano
Department of Metallurgical Engineering
Case Institute of Technology
Cleveland 6, Ohio

76
Professor W. W. Webb
Department of Engineering Physics
Cornell University
Ithaca, New York

77
Dr. J.C.M. Li
Edgar C. Bain Research Laboratory
U. S. Steel Corporation
Monroeville, Pennsylvania

78
Dr. R. L. Smith
The Franklin Institute
Philadelphia 3, Pennsylvania

79
Dr. H. S. Rosenbaum
Research Laboratories
General Electric Corporation
Schenectady, New York

80
Dr. W. G. Johnston
Research Laboratories
General Electric Corporation
Schenectady, New York

81
Professor T. A. Read
Department of Mining and Metallurgy
University of Illinois
Urbana, Illinois

82
Professor P. A. Beck
Department of Mining and Metallurgy
University of Illinois
Urbana, Illinois

83
Professor P. Gordon
Department of Metallurgical Engineering
Illinois Institute of Technology
Chicago 16, Illinois

84
Professor B. L. Averbach
Department of Metallurgy
Massachusetts Institute of Technology
Cambridge 39, Massachusetts

Copy Number — Distribution List - Cont'd

85
Professor E. Katz
Department of Physics
University of Michigan
Ann Arbor, Michigan

86
Professor M. E. Nicholson
Department of Metallurgy
University of Minnesota
Minneapolis 14, Minnesota

87
Professor G. C. Kuczynski
Department of Metallurgy
University of Notre Dame
Notre Dame, Indiana

88
Professor J. W. Spretnak
Department of Metallurgy
Ohio State University
Columbus, Ohio

89
Dr. C. Zener
Westinghouse Electric Corporation
Research Laboratories
Beulah Road
Churchill Borough
Pittsburgh 13, Pennsylvania

90
Institute for the Study of Metals
University of Chicago
Chicago, Illinois
Attn: Dr. C. S. Barrett

91
Professor J. J. Gilman
School of Applied Mathematics
Brown University
Providence, Rhode Island

92
Professor Peter Gibbs
Institute for the Study of Rate Processes
University of Utah
Salt Lake City, Utah

93
Professor Norman Brown
University of Pennsylvania
Philadelphia, Pennsylvania